Theoretical and Applied Fracture Mechanics 131 (2024) 104386

Contents lists available at ScienceDirect

Theoretical and Applied Fracture Mechanics

journal homepage: www.elsevier.com/locate/tafmec

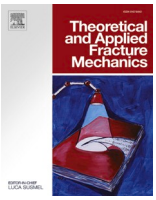

Meshfree simulation of dynamic brittle and quasi-brittle fracture using a local damage model based on lattice particle method

K.C. Ng [a,*], Hailong Chen [b], W.C. Low [a]

[a] Department of Mechanical, Materials and Manufacturing Engineering, University of Nottingham Malaysia, Jalan Broga, 43500 Semenyih, Selangor Darul Ehsan, Malaysia
[b] Department of Mechanical and Aerospace Engineering, University of Kentucky, Lexington, KY 40506, USA

ARTICLE INFO

Keywords:
Dynamic fracture
Meshfree models
Lattice Particle Method (LPM)
Local damage model
Isotropic damage model
Lattice Spring Model (LSM)

ABSTRACT

In this paper, the particle size-dependent issue of Lattice Particle Method (LPM) for simulating dynamic brittle and quasi-brittle fracture is addressed by coupling LPM with a local damage model based on fracture energy. The proposed model is simple and more robust than the Stress Intensity Factor (SIF)-based approach as it can model mixed-mode fracture with multiple cracks without any application-dependent tuning parameter. Numerical procedures for estimating the dissipative energy and the crack tip velocity for LPM simulation are also proposed. A series of benchmark problems involving dynamic fracture and crack branching are simulated using the proposed model. Good agreements are found against existing experimental observation and solutions from other numerical methods. Although a Cartesian-like (structured) lattice configuration is employed in the current LPM method, physically meaningful and accurate crack patterns can still be captured without any special numerical treatment.

1. Introduction

Due to its practical relevance in technology and an inherent scientific inquisitiveness, dynamic fracture in solid materials has been a subject of significant interest amongst engineers and scientists for more than a century. Under extreme dynamic conditions, forces applied at high rate either intentionally or accidentally, are encountered in numerous practical applications such as mining, blasting, natural disasters (e.g., flooding, tsunami), etc. Irrespective of the nature of these high-rate loadings, it is essential to comprehend the mechanisms and principles governing material failure under dynamic loadings. This understanding is crucial for designing effective procedures to assess susceptibility to material failure subject to dynamic loadings [1].

Traditionally, physical experiments [2,3] have been conducted to understand the mechanisms of dynamic fracture. Unfortunately, experimentation in the field of dynamic fracture is very challenging due to many technical complications such as short duration of the event, lack of reproducibility and scaling issues, etc. Therefore, performing numerical simulation using validated numerical models to study complex crack propagation under dynamic loading is a common practice nowadays and various numerical techniques have been developed so far.

Due to its predominant application for continuous problems, mesh-based methods such as the Finite Element Method (FEM) has been widely applied to model dynamic fracture in solid bodies. In general, there are two major crack modelling techniques proposed in most of the FEM studies, i.e., the discontinuous (sharp) method and the smeared (diffusive) method. The discontinuous approach, such as the popular Extended-Finite Element Method (XFEM) [4], permits the passage of crack paths through finite elements. While discontinuous approach can represent a crack sharply using some crack tracking algorithms, monitoring the development of intricate fractured surfaces particularly in three-dimensional (3D) scenarios is undoubtedly a challenging and computationally intensive undertaking. The smeared method, on the other hand, does not require tracking of fractured surfaces algorithmically. Instead, a specific form of damage function is solved and the elements with damage values above a certain threshold are used to represent the crack path. Therefore, it has been regarded as a more practical model for large scale simulation due to its computational simplicity [5,6].

In general, there are two types of smeared cracking model, i.e., local and non-local damage models, where different regularization techniques have been employed to address the mesh size dependency problem. Non-local damage model typically requires the solution of non-local stress/strain, either by using additional Partial Differential Equation

* Corresponding author.
E-mail addresses: khaiching.ng@nottingham.edu, ngkhaiching2000@yahoo.com (K.C. Ng).

https://doi.org/10.1016/j.tafmec.2024.104386
Received 26 October 2023; Received in revised form 17 February 2024; Accepted 18 March 2024
Available online 20 March 2024

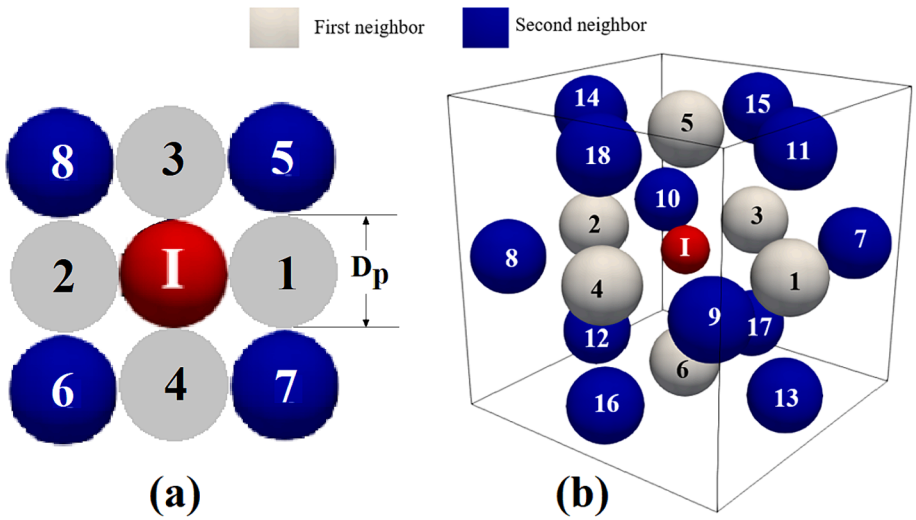

Fig. 1. (a) 2D square lattice and (b) 3D simple cubic lattice in LPM [41]. D_p is particle size/diameter. The centre-to-centre distances between local particle I and its first and second neighbours are D_p and $\sqrt{2}D_p$, respectively.

(PDE) that must be solved via the gradient-enhanced non-local model [7,8] or by performing weighted averaging of the neighboring local equivalent stress/strain via the integral non-local model [9,10]. While the issue of mesh size dependency can be resolved at the expense of extra computational cost, non-local damage models typically require a denser mesh particularly in the damaged region. In fact, the nature of those popular phase field models [11,12] is quite similar to that of non-local model, where the PDE of the phase field variable is solved. Interestingly, a recent study [13] has pointed out that phase field models tend to overestimate the dissipative energy. For local damage models, regularization techniques such as the crack band model [14], the cohesive crack model [15] and the fracture mechanics-based model [16] can be introduced to address the mesh size dependency issue. The major strength of local model is its ability in capturing complex crack paths at low computational cost (without solving any evolution equations) and no ad-hoc criteria is needed for crack growth [13]. Nevertheless, local models suffer from mesh bias issue in FEM and hence coupling with other advanced methods (hence extra computational cost) such as crack-tracking algorithm [17] and non-local strain averaging [18] are required to address this problem.

On the other hand, meshfree models have gained significant popularity for simulating dynamic fractures due to the elimination of mesh-related issues. In Peridynamics (PD), particles within the radius of influence (or horizon) interact in a pair-wise manner and their motions are governed by integro-differential equations. There is no PDE involved in PD; hence, it is very suitable for simulating crack propagation problems [19,20] as spatial derivatives are undefined at discontinuity. The bond between a PD particle pair is broken if its elongation exceeds a critical value that is determined by the horizon size and the material fracture energy [21]. Smoothed Particle Hydrodynamics (SPH) works in a somewhat similar manner as PD where two particles within certain radius of influence mutually interact. However, unlike PD, SPH still employs differential equations where spatial derivatives are formulated in the form of weighted kernel summation. In SPH, dynamic fracture can be handled by breaking the pseudo-spring or energy bond between the interacting particles [22,23]. Another popular classical meshfree method known as the Discrete Element Method (DEM) has also been used to simulate brittle fracture in both quasi-static and dynamic conditions [24,25]. Typically, a DEM particle interacts with its nearest neighbors in a pair-wise manner and DEM might work only for a limited range of Poisson's ratio. Different from DEM, Lattice Spring Models (LSM) that can handle a wider range of Poisson's ratio have been developed, e.g., the Distinct LSM [26], the four-dimensional LSM [27], and the Lattice Particle Method (LPM) (or previous known as Volume Compensated Particle Method (VCPM)) [28]. LSM also involves pair-wise interactions between immediate neighboring particles, which are typically short-ranged. To simulate a wider range of Poisson's ratio in LSM, non-local term is introduced by considering integral effect of all neighbors or using multi-body lateral (or shear) springs. According to Pan and co-workers [29], most of the failure criteria employed in LSM are critical stress (force) criterion [30,31], and critical strain (displacement) criterion [23,32,33]. Unfortunately, the numerical results are highly dependent on the particle size, and other criteria based on fracture energy could be implemented to address the issue. For a more comprehensive review on meshfree methods for fracture modelling, readers are referred to Refs. [29,34].

Some strategies have been implemented recently in addressing the particle size dependency issue using the LPM. Meng and Liu [33] introduced smoothing technique for the local damage parameter by incorporating the damage information of neighboring particles in a way similar to the integral nonlocal damage model. While this approach can address the particle size dependency issue, it is necessary to incorporate the characteristic length scale and the critical bond damage threshold (for bond breaking purpose), where calibrations are needed for different cases. Recently, Ng and Chen [35] have modelled the brittle fracture using LPM by calculating the Stress Intensity Factor (SIF) near the crack tip. Bond breaking is performed if the computed particle's SIF value exceeds the fracture toughness of the material. Although the method has been successfully extended to simulate Fluid Structure Interaction (FSI) problems without mesh dependency issue, it is limited to mode-I fracture and hence complex crack patterns cannot be simulated accurately.

In the current work, the main objective is to develop a more robust damage model for LPM in handling problems involving complex mixed-mode fractures under dynamic loadings. Emphasis is paid to incorporating the local damage model based on fracture energy into LPM to simulate dynamic fracture for brittle and quasi-brittle materials. The force formulation in LPM is modified accordingly by incorporating the damage parameter in both the local and non-local terms. Techniques used to estimate the crack tip speed and the dissipative energy for LPM are formulated as well. To verify the proposed method, four numerical experiments involving dynamic fracture and crack branching are modelled and results are compared against experimental observations and numerical solutions using other models. The paper concludes with some potential implementations that could be considered for improving the current work.

Table 1
The bond stiffness in terms of material properties for 2D square and 3D simple cubic lattices in LPM. Young's modulus, Poisson's ratio, material thickness and particle size are represented by E, υ, t_h and D_p, respectively.

Model	k_1	k_2	T
2D plane stress	$\frac{2Et_h}{1+\upsilon}$	$\frac{Et_h}{1+\upsilon}$	$\frac{Et_h(3\upsilon-1)}{2(1+\upsilon)(1-\upsilon)(1+\sqrt{2})^2}$
2D plane strain	$\frac{2Et_h}{1+\upsilon}$	$\frac{Et_h}{1+\upsilon}$	$\frac{Et_h(4\upsilon-1)}{(1+\upsilon)(1-2\upsilon)(2+\sqrt{2})^2}$
3D	$\frac{ED_p}{1+\upsilon}$	$\frac{ED_p}{1+\upsilon}$	$\frac{ED_p(4\upsilon-1)}{2(1+\upsilon)(1-2\upsilon)(1+2\sqrt{2})^2}$

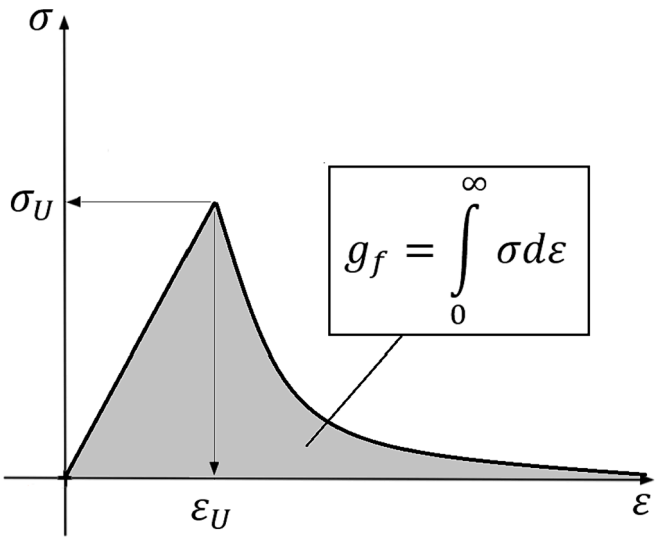

Fig. 2. A typical stress–strain curve involving material softening.

2. Mathematical models and numerical methods

2.1. Brief review of lattice particle method (LPM)

The Lattice Particle Method (LPM) (or Volume Compensated Particle Method (VCPM) [28,36]) is a meshfree method originally developed by Chen and co-workers [28] for modelling solid mechanics problems such as those involving solid fracture [33,36] and Fluid Structure Interaction (FSI) [35,37,38,39]. By reformulating the classical continuum mechanics model using discretized integro-differential equations, LPM solves the numerical issues in continuum mechanics-based models for discontinuous problems, such as crack tip singularity issue. Fig. 1 shows the 2D square lattice and 3D simple-cubic lattice used in LPM, where a solid particle I interacts with its first and second neighbouring particles J via bonds (with certain values of local stiffness k and non-local volumetric stiffness T [28]).

The motion of a solid particle I follows the Newton second law as:

$$m_I\frac{d\mathbf{v}_I}{dt}=\mathbf{F}_{S,I}, \tag{1}$$

where m_I is mass of particle I, $\mathbf{v}_I$ is the velocity of particle I, and $\mathbf{F}_{S,I}$ is the net force acting on the particle I from all its neighbours J that can be determined as:

$$\mathbf{F}_{S,I}=\sum_J f_{IJ}\hat{\mathbf{u}}_{IJ}, \tag{2}$$

where $\hat{\mathbf{u}}_{IJ}=(\mathbf{r}_I-\mathbf{r}_J)/\|\mathbf{r}_I-\mathbf{r}_J\|$ is the unit bond vector and f_{IJ} is the bond force. In the current work, the damage incurred to an elongated half-bond connected to the local particle I is modelled by multiplying the force of the half-bond by a factor of $(1-D_I)$, where D_I is the local damage parameter of particle I. In fact, the above procedure is equivalent to that of multiplying the bond stiffness values by $(1-D_I)$ as implemented by Choo and co-workers [40]. The value of damage parameter D ranges between 0 (undamaged) and 1 (fully damaged) and its modelling is further explained in the following section. By performing the same procedure on another half-bond connected to the neighbouring particle J and taking the arithmetic mean of these two half-bond forces to ensure momentum conservation, we obtain:

$$f_{IJ}=\underbrace{-(1-D_{IJ})k\delta l_{IJ}}_{\text{local}}\underbrace{-\frac{T}{2}\left(\sum\nolimits_Q(1-D_I)\delta l_{IQ}+\sum\nolimits_M(1-D_J)\delta l_{JM}\right)}_{\text{non-local}}, \tag{3}$$

where $D_{IJ}=(D_I+D_J)/2$. δl_{IJ} takes the value of half-bond elongation between particles I and J. The subscripts Q and M indicate the neighbours of particles I and J, respectively. The bond stiffness values k and T can be determined by ensuring energy equivalency between the LPM description and its continuum counterpart [32]. The stiffness values of k and T are tabulated in Table 1 for different models. Note that the subscripts 1 and 2 of bond stiffness k refer to the first and the second neighbours (see Fig. 1), respectively.

2.2. Isotropic local damage modelling

For modelling the non-linear behaviour of quasi-brittle material using LPM, the isotropic damage model is implemented where its softening behaviour is monitored through a scalar (directionally independent) parameter D, or better known as the damage parameter. The constitutive equation is redefined as:

$$\sigma_{ij}=(1-D)\sigma^o_{ij}=(1-D)C_{ijkl}\varepsilon_{kl}, \tag{4}$$

where σ_{ij} is the stress tensor, $\sigma^o_{ij}=C_{ijkl}\varepsilon_{kl}$ is the undamaged stress tensor, C_{ijkl} is the material stiffness tensor and ε_{kl} is the strain tensor. The damage parameter is typically 0 (undamaged) in the elastic regime and it is within the range (0,1] in the softening (non-linear) regime.

From the literature, various ways can be used to define the damage function in the softening regime, e.g., linear [42,43], exponential [6,16,42,44], etc. In the current work, we adopt the exponential approach where D is expressed as [42]:

$$D=\begin{cases}0, \sigma^t\le\sigma_U\\ 1-\dfrac{\sigma_U}{\sigma^t}e^{-2H_S\left(\frac{\sigma^t-\sigma_U}{\sigma_U}\right)}, \sigma^t>\sigma_U\end{cases}, \tag{5}$$

where σ^t is the maximum equivalent stress in the deformation time history, i.e., $\sigma^t=\max(\sigma_{eq}(t))$, σ_U is the material strength and H_S is a positive constant to be determined from the uniaxial tension test as discussed below.

Like being used in FEM, we assume that the bandwidth of the damaged zone in LPM is concentrated within a unit cell of certain characteristic length l^*, which is dependent on the particle size D_p. This characteristic length could be calibrated accordingly [44] in order to reproduce the specified fracture energy in a given problem. The detail of the calibration procedure is discussed later. The area under the respective stress–strain curve depicted in Fig. 2 is indeed the total specific dissipative energy (energy per unit volume) represented by g_f. This specific dissipative energy is related to the fracture energy G_f [14] as:

$$g_f=\frac{G_f}{l^*}. \tag{6}$$

By combining Eqs. (4) and (5), the stress–strain relationship for 1D problem can be written as:

$$\sigma=(1-D)E\varepsilon=\begin{cases}E\varepsilon, \varepsilon\le\varepsilon_U\\ E\varepsilon_U e^{-\beta(\varepsilon-\varepsilon_U)}, \varepsilon>\varepsilon_U\end{cases}, \tag{7}$$

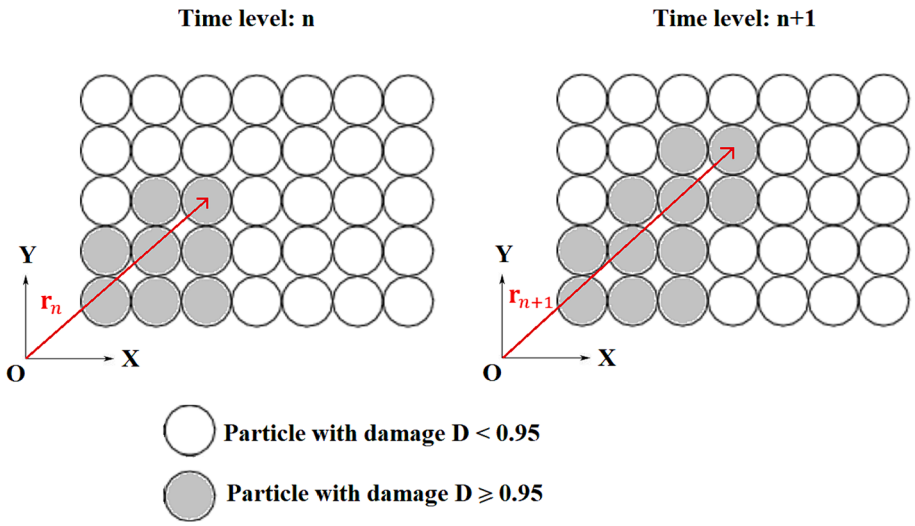

Fig. 3. Scheme for tracking crack tip in LPM.

upon defining $\beta = 2H_S/\varepsilon_U$, $\sigma^t = E\varepsilon$ and $\sigma_U = E\varepsilon_U$. Here, β is typically known as softening parameter in literature. From Fig. 2, the specific dissipative energy can be evaluated as:

$$g_f = \int_0^\infty \sigma d\varepsilon = \frac{1}{2}E\varepsilon_U^2 + \frac{1}{\beta}E\varepsilon_U = \frac{G_f}{l^*}. \tag{8}$$

Rearranging terms in Eq. (8), it can be shown that:

$$\beta = \frac{E\varepsilon_U l^*}{G_f - \frac{1}{2}E\varepsilon_U^2 l^*}. \tag{9}$$

It is important to note that Eq. (9) is the form of softening parameter β reported in Ref. [13]. By noting $\beta = 2H_S/\varepsilon_U$ and making use of Eq. (9), the definition of H_S by Cervera and Chiumenti [42] can be recovered accordingly as:

$$H_S = \frac{\widetilde{H_S} l^*}{1 - \widetilde{H_S} l^*}, \tag{10}$$

where $\widetilde{H_S} = \sigma_U^2/(2G_f E)$. Other researchers [6,45] have further introduced a constant parameter A and defined it as $A = 2H_S$. From this definition, it is straightforward to show that $A = \left(\frac{G_f E}{l^* \sigma_U^2} - \frac{1}{2}\right)^{-1}$, thus reproducing the parameter A reported earlier by [6,45]. As H_S must be positive, based on Eq. (10): $l^* < \frac{1}{\widetilde{H_S}} = \frac{2G_f E}{\sigma_U^2}$, which would limit the maximum particle size in the LPM simulation. To correctly reproduce the specified value of fracture energy using LPM, we have computed the fracture energy of a specimen (with known fracture energy) with different initial notch lengths from the simulated force–displacement curves obtained from the three-point bending test (see Li's method [46]). After some sensitivity studies, it is found that the specified fracture energy for 2D problem can be reproduced at reasonable accuracy when $l^* \sim D_p$ where D_p is the particle size. For 3D problem, $l^* \sim D_p$.

2.3. Estimation of dissipative energy and crack tip speed

Inspired by the work in Ref. [13], a method has been devised to estimate the crack tip location/speed by identifying the fully damaged particles. Following Ref. [13], a particle is considered as fully damaged if $D \geq 0.95$. For each time step, the position vector of the farthest fully damaged particle $\mathbf{r}$ is identified, as shown in Fig. 3. The crack tip speed $v_{c,n+1}$ at time step n + 1 is then computed as:

$$v_{c,n+1} = \frac{\Delta l_{n+1}}{t_{n+1} - t_n} = \frac{\|\mathbf{r}_{n+1} - \mathbf{r}_n\|}{t_{n+1} - t_n}, \tag{11}$$

where Δl is the distance travelled by the crack tip within a certain time step size. Accordingly, the total dissipative energy per unit depth, U_d during the entire fracturing process can then be calculated as:

$$U_d = G_f \sum_{n=0}^{N-1} \Delta l_{n+1} = G_f \sum_{n=0}^{N-1} \|\mathbf{r}_{n+1} - \mathbf{r}_n\|, \tag{12}$$

where N is the total number of time steps. The current method of estimating the dissipative energy based on crack length is analogous to that of the cracking node method of Song and Belytschko [47]. Note that Eq. (12) is valid only for 2D problems of constant thickness.

2.4. Time integration

In the current work, the equation of motion (Eq. (1)) is integrated using the predictor–corrector scheme detailed in our previous work [48]. It is briefly discussed here.

Step 1: By using Eq. (1), the acceleration $\left(\frac{d\mathbf{v}_I}{dt}\right)^m$ of solid particles I is computed. Its velocity $(\mathbf{v})$ and displacement $(\mathbf{r})$ vectors at intermediate time step $m+0.5$ are predicted as:

$$\mathbf{v}_I{}^{m+0.5} = \mathbf{v}_I{}^m + \frac{\Delta t}{2}\left(\frac{d\mathbf{v}_I}{dt}\right)^m, \tag{13}$$

$$\mathbf{r}_I{}^{m+0.5} = \mathbf{r}_I{}^m + \frac{\Delta t}{2}\mathbf{v}_I{}^m. \tag{14}$$

Here, m is the time step counter and Δt is the time step size, which is bounded to the stability criterion [37]:

$$\Delta t < 0.8\frac{D_p}{c_S}, \tag{15}$$

where c_S is the sound speed in the solid body.

Step 2: Based on the intermediate velocity and displacement vectors computed from Step 1, the acceleration of solid particle I, i.e., $\left(\frac{d\mathbf{v}_I}{dt}\right)^{m+0.5}$ is recalculated again using Eq. (1). Next, the velocity and displacement vectors of solid particle I at t^{m+1} are corrected as:

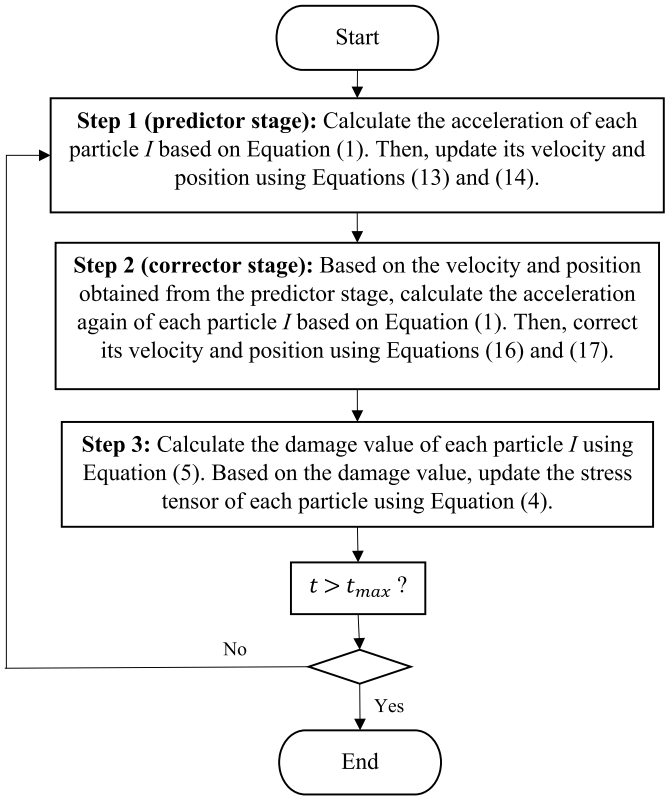

Fig. 4. Flow chart of the current numerical procedure using the explicit predictor–corrector integration scheme. t_{max} is the user-specified maximum simulation time.

$$\mathbf{v}_I^{m+1} = \mathbf{v}_I^m + \Delta t \left(\frac{d\mathbf{v}_I}{dt}\right)^{m+0.5}, \tag{16}$$

$$\mathbf{r}_I^{m+1} = \mathbf{r}_I^m + \frac{\Delta t}{2}\left(\mathbf{v}_I^m + \mathbf{v}_I^{m+1}\right). \tag{17}$$

Step 3: At this stage, the damage value of each particle is calculated using Equation (5). In the current work, the equivalent stress is calculated using the standard Rankine criterion, i.e., $\sigma_{eq} = \langle \sigma_1^o \rangle$ where $\langle \blacksquare \rangle = \frac{|\blacksquare|+\blacksquare}{2}$ is the Macauley bracket and σ_1^o is the maximum principal stress of the undamaged Cauchy stress tensor σ_{ij}^o. The Cauchy stress tensor of solid particle I is calculated as [33,49]:

$$\sigma_{ij}^o = -\frac{1}{V}\sum_J L_{IJ} f_{IJ} n_i^J n_j^J, \tag{18}$$

where V is the particle volume, L_{IJ} is the original half-length of the bond connecting solid particle I and its neighbour J, f_{IJ} is the bond force magnitude at undamaged state (setting $D = 0$ in Eq. (3)), n_i^J and n_j^J are the i- and j-components of the unit vector pointing from solid particle I to its neighbour J, respectively. To improve the accuracy of the stress computation at the boundary, the corrective approach suggested by Meng and co-workers [50] is adopted. Once the damage value is computed, the stress tensor of each particle can then be updated using Eq. (4).

The detail of the above numerical procedure is outlined in Fig. 4.

3. Result and discussion

In this section, the accuracy of the proposed damage model for LPM is tested by simulating a series of cases involving dynamic fracture and crack branching. Numerical results including crack pattern, crack tip speed and dissipative energy are compared against experimental observation and numerical data available from open literature. Unless mentioned otherwise, plane stress conditions are assumed for the two-dimensional problems considered in the current work.

3.1. Dynamic fracture in the Kalthoff-Winkler experiment

The brittle fracture observed in the Kalthoff-Winkler experiment [3] has been previously simulated using various numerical methods [36,47,51]. The geometric configuration of this problem is shown in Fig. 5. In this example, a thin plate made of maraging steel 18Ni1900 (Young's modulus $E = 190$ GPa; Poisson's ratio $\upsilon = 0.3$; density $\rho = 8000$ kg/m^3; material strength $\sigma_U = 1.9$ GPa; fracture energy $G_f = 22130$ J/m^2) with two initial notches is impacted by a projectile moving at $v_o = 16.5$ m/s [13]. From the experimental study [3,52], brittle fracture is observed, and the cracks propagate at $\sim 70^\circ$ (measured from the horizontal axis) at this relatively low impact speed.

Following [11,13], the impact of the projectile is modelled by prescribing the horizontal velocity U (see Fig. 5) as a time-varying function:

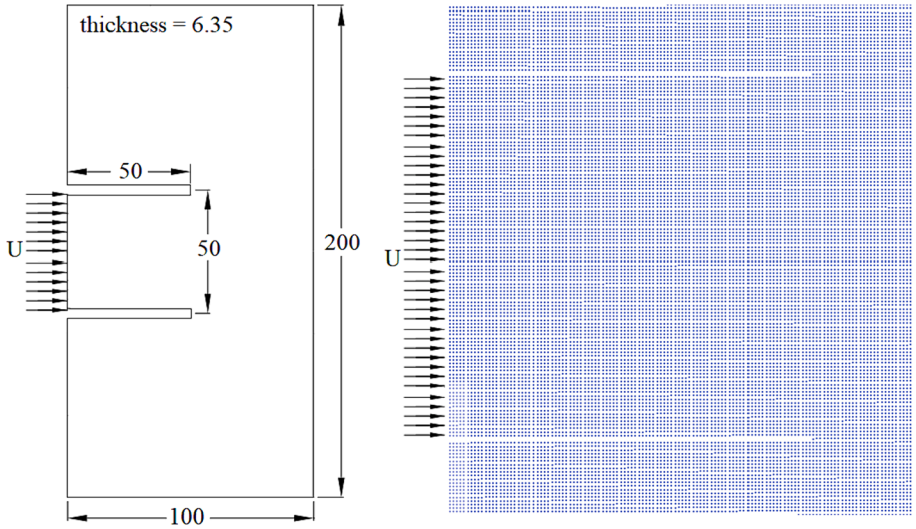

Fig. 5. Geometry of notched plate used in the Kalthoff-Winkler experiment and the discretized model using LPM (Dimensions in mm).

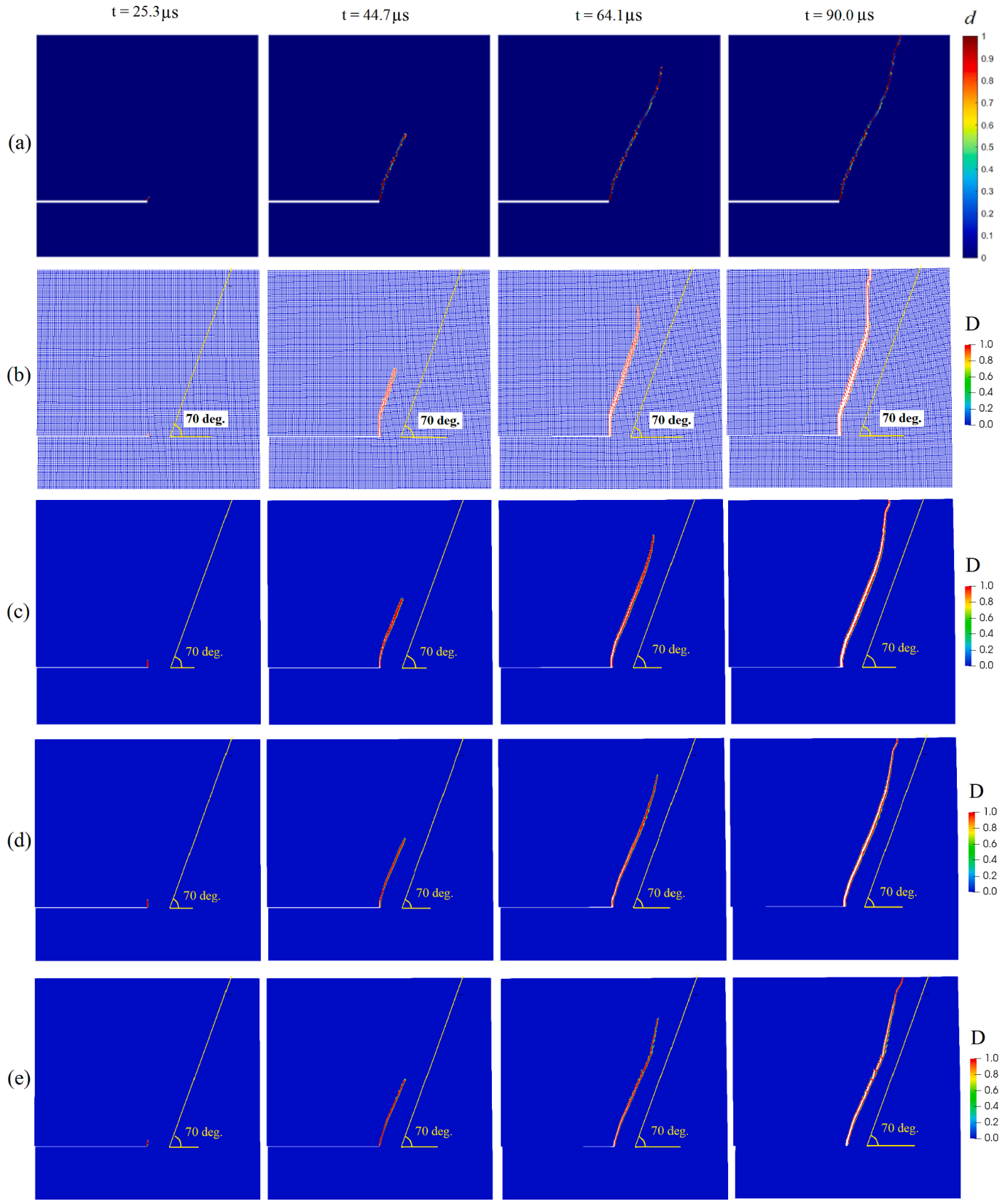

Fig. 6. Damage field evolution predicted using (a) FEM [13]; (b) LPM (D_p = 0.5 mm); (c) LPM (D_p = 0.25 mm); (d) LPM (D_p = 0.125 mm) and (e) LPM (D_p = 0.0625 mm).

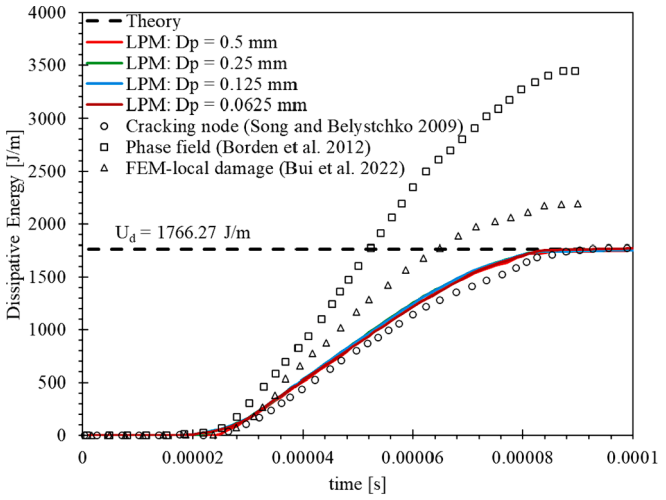

(a)

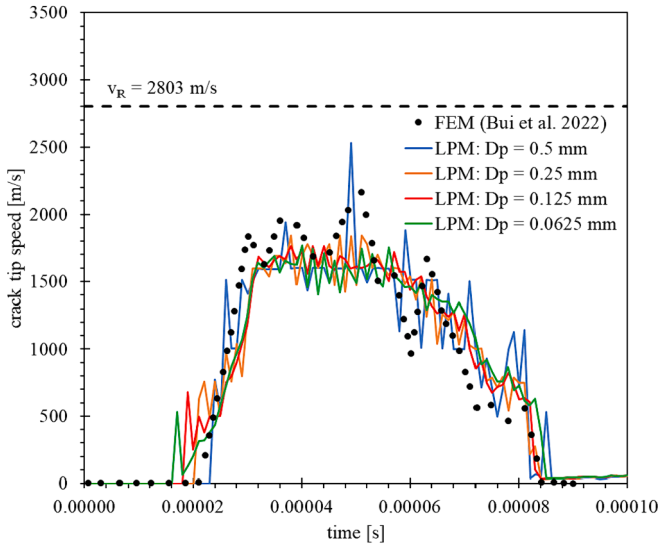

(b)

Fig. 7. Effect of LPM particle size on the (a) dissipative energy per unit depth and (b) crack tip speed of the upper crack for the Kalthoff-Winkler dynamic brittle fracture case.

$$U = \begin{cases} \frac{t}{t_o} v_o, t < t_o \\ v_o, t \geq t_o \end{cases}, \tag{19}$$

where $t_o = 1$ μs. In contrast with most of the existing studies where only half plate is considered due to symmetry [23,47], the entire plate is modelled in the current work, and it is confirmed that the simulated crack pattern is indeed symmetrical. As discussed previously [19,35,53], either Remove Bond (RB) or Remove Particle (RP) approach could be used to model a notch. Due to the natures of the loading condition and the notch location, the upper and lower edges of a notch would come in contact (leading to penetration) at the later stage of the simulation if RB is used. To address this problem, a collision detection algorithm could be employed; however, this is beyond the scope of the current study. Hence, one layer of particles is removed to model the notch using the RP method following [53] (see Fig. 5). Different particle sizes are used to test the convergence of the current method.

Fig. 6 shows the predicted crack propagation in the plate. The damage function (D) (see Fig. 6 (b–e)) indicates that a small crack starts to grow from the notch tip at $t \sim 25$ μs. It is appealing to note that its

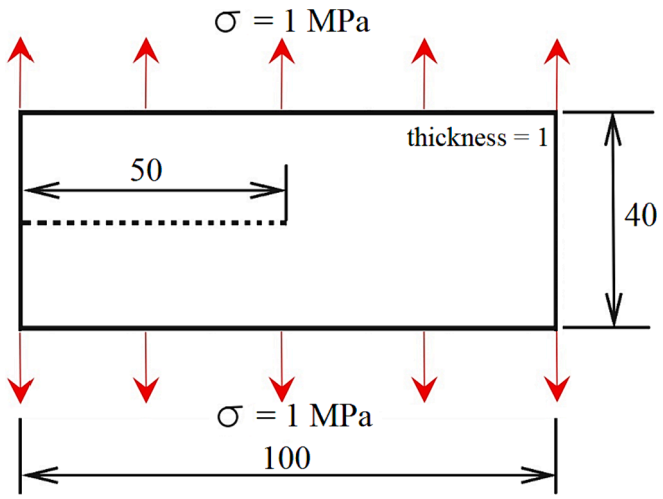

Fig. 8. Geometry and configuration of the dynamic crack branching problem. The dashed line indicates initial notch. Dimensions in mm.

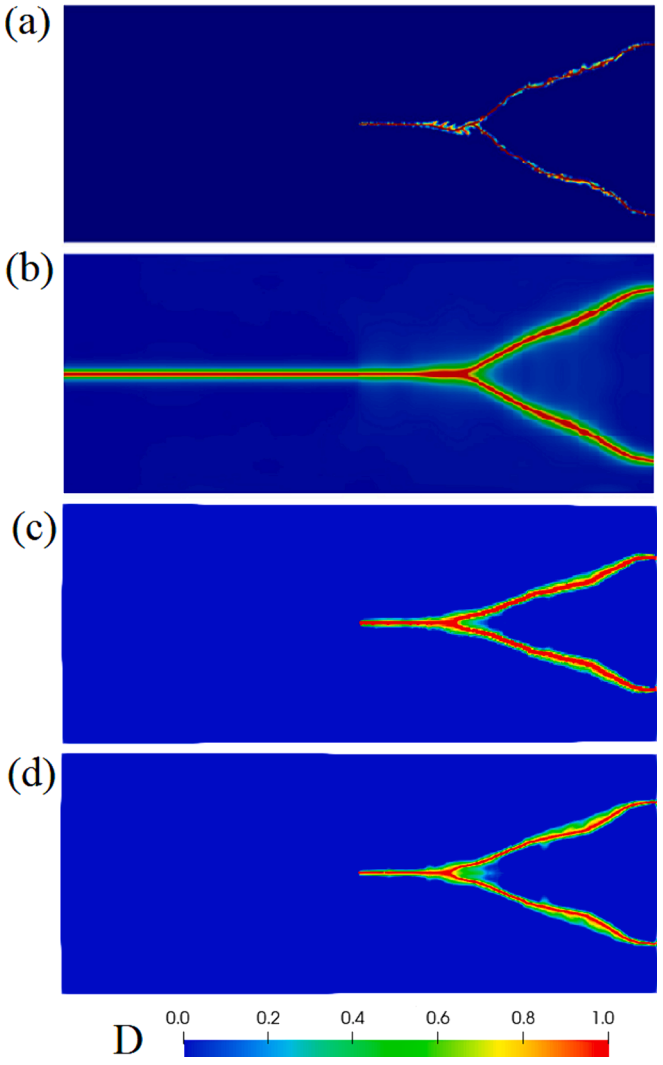

Fig. 9. Comparison of crack paths predicted using (a) FEM-local damage model with locally refined unstructured mesh of size ~0.3 mm [13]; (b) Phase field model [11] with mesh spacing 0.0625 mm; (c) LPM ($D_p = 0.25$ mm); and (d) LPM ($D_p = 0.125$ mm). The colour legend is meant for (c) and (d).

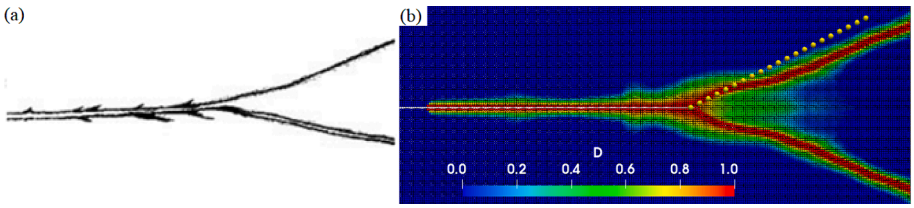

Fig. 10. Comparison of crack path with experiment. (a) Experiment [2]; (b) LPM ($D_p = 0.125$ mm). The yellow dotted line shows the theoretical crack angle of 27° measured from the horizontal line. (For interpretation of the references to colour in this figure legend, the reader is referred to the web version of this article.)

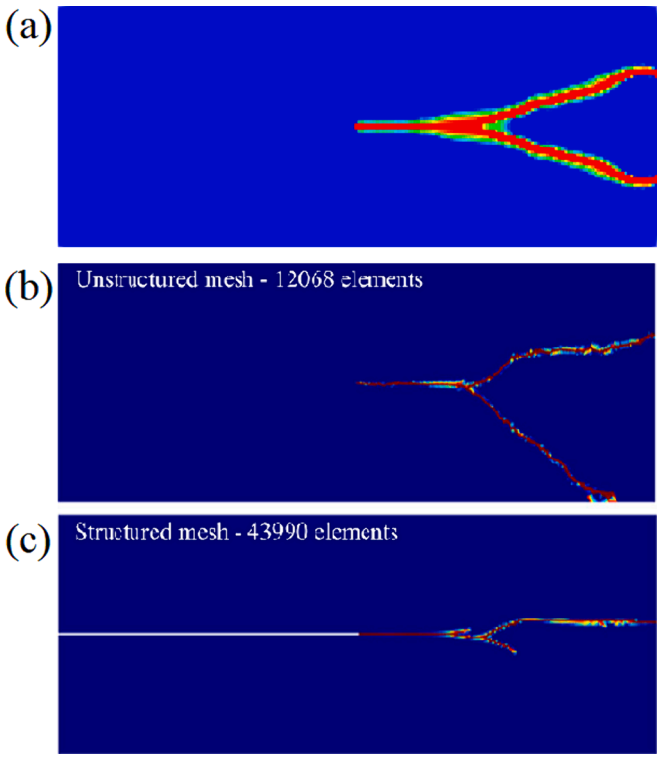

Fig. 11. Crack paths simulated using (a) the LPM model with relatively coarse particle spacing of $D_p = 0.5$ mm (16,000 particles) and the FEM-local damage model of Bui et al. [13] by employing (b) unstructured mesh (size of 0.5 mm; 12,068 elements) and (c) structured mesh (size of 0.2 mm; 43,990 elements).

propagation angle is quite consistent with that observed experimentally (~70°) during the first 64 μs. Nevertheless, as the crack approaches the top surface, the propagation angle increases, which is consistent with other numerical observations reported earlier [47,54]. The crack patterns at different time levels obtained using LPM models of various particle resolutions have been compared against those from FEM [13] as shown in Fig. 6. It is found that the agreement is encouraging. The current simulation results clearly demonstrate the ability of LPM in capturing the brittle fracture.

The estimated dissipative energies per unit depth obtained from LPM simulation are plotted in Fig. 7(a) for different particle sizes. As can be seen, the effect of particle size on the simulated dissipative energy is not

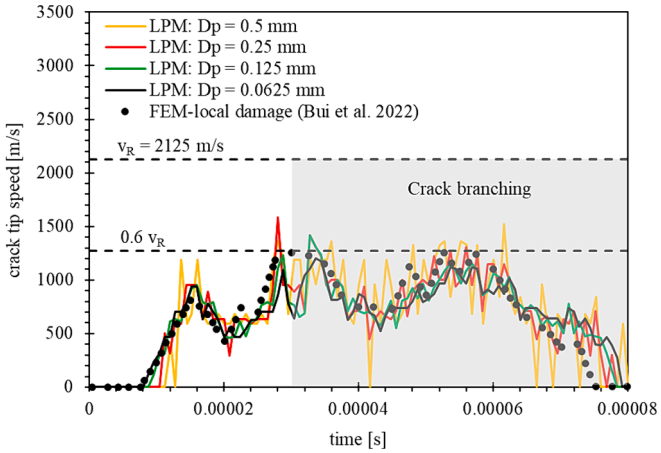

Fig. 13. Comparison of crack tip speeds predicted using different methods. Upon branching, the speed of the top branch is shown.

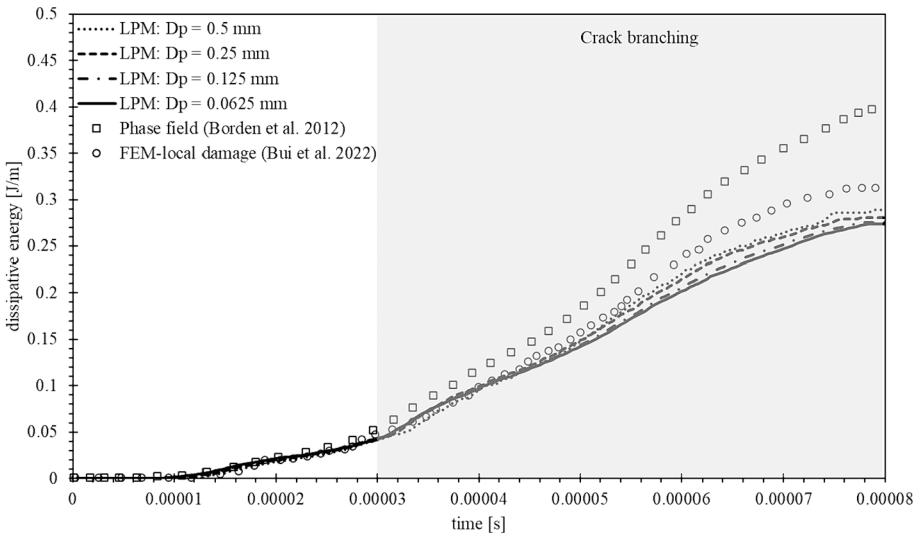

Fig. 12. Dissipative energy per unit depth for the crack branching problem predicted using different methods.

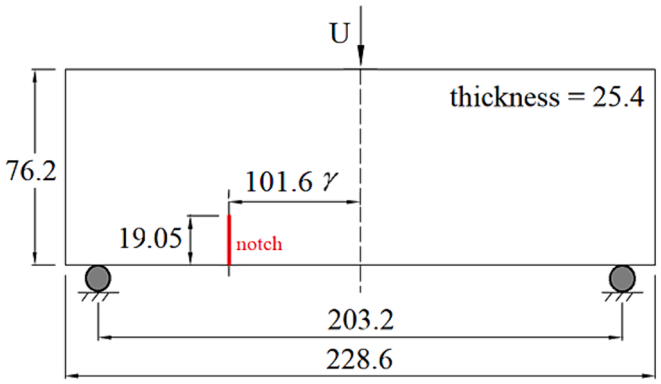

Fig. 14. Geometrical details of the three-point bending experimental setup of John and Shah [57]. Dimensions in mm.

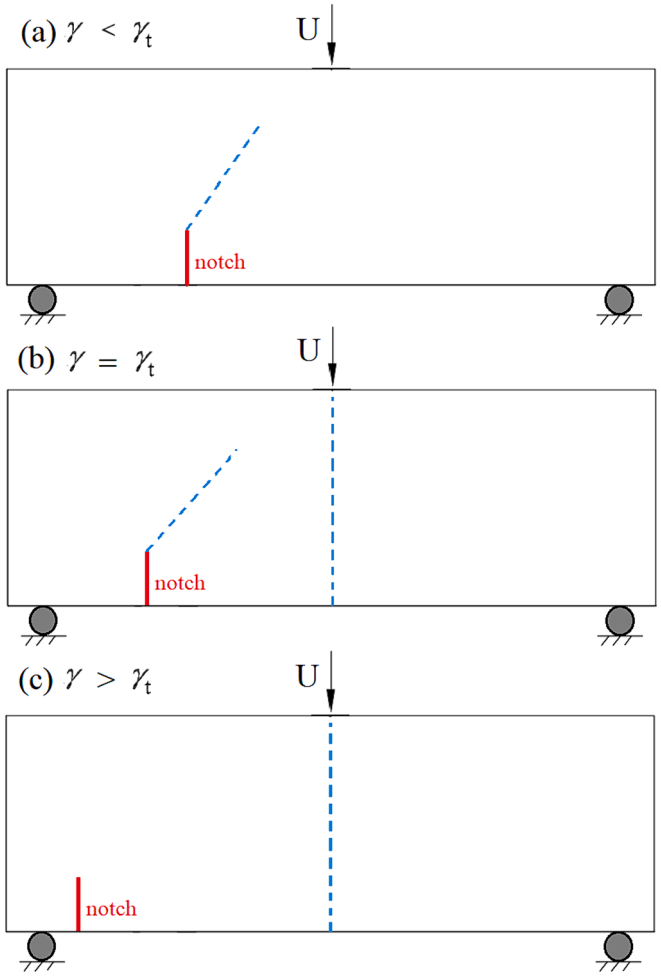

Fig. 15. Possible crack paths (shown in blue dashed lines) of the three-point bending experimental setup of John and Shah [57] due to different notch locations. (For interpretation of the references to colour in this figure legend, the reader is referred to the web version of this article.)

apparent. More convincingly, like the cracking node method [47], the dissipative energies estimated using different LPM particle sizes converge to the theoretical solution of $U_d = 1766.27$ J/m, which could be attributed to the fact that the simulated crack angle is quite close to that observed experimentally (i.e., 70°). It is noted that the theoretical solution is obtained from the theoretical crack length (assuming the crack is perfectly linear) for the ideal case where the crack propagates at

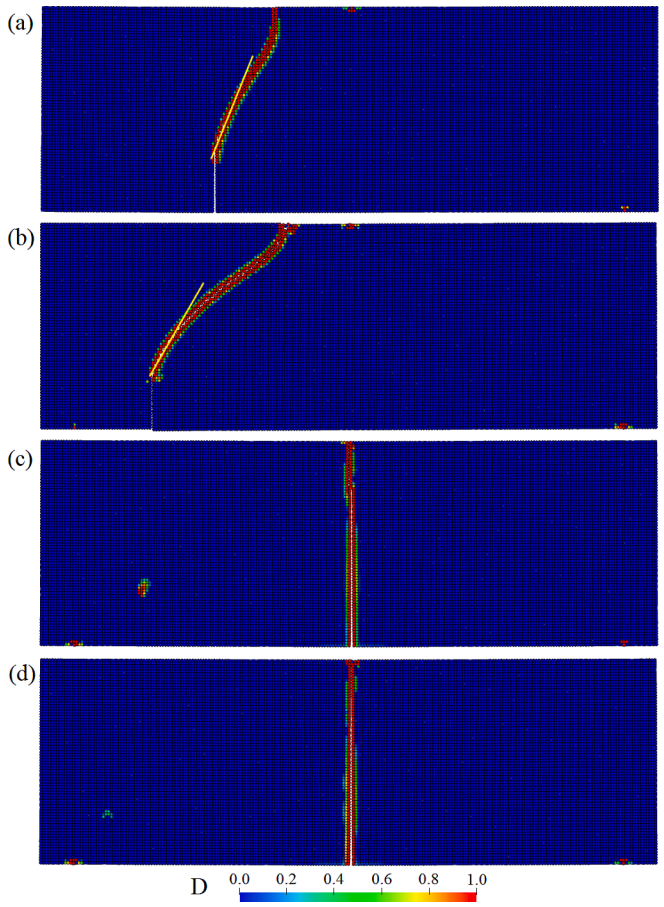

Fig. 16. Crack patterns at notch positions predicted using LPM. (a) $\gamma = 0.5$; (b) $\gamma = 0.72$; (c) $\gamma = 0.76$ ($=\gamma_t$) and (d) $\gamma = 0.875$. The crack directions (represented by yellow solid lines) predicted using LEFM for (a) and (b) are 22° and 30° (measured from the vertical axis), respectively. (For interpretation of the references to colour in this figure legend, the reader is referred to the web version of this article.)

70° from the horizontal axis [13]. As the dissipative energies calculated by the current approach (Eq. (12)) and the cracking node method [47] are based on crack length, the estimated dissipative energies should be closed to the theoretical value if the crack length (or crack angle) is estimated accurately. The FEM solution [13] is slightly higher than the theoretical solution due to the smaller crack propagation angle (65°-66°) that translates to larger crack length.

Next, the crack tip velocities predicted using different LPM particle sizes are compared against those of FEM [13] in Fig. 7(b). The crack tip velocity is generally insensitive to the LPM particle size, except for the relatively coarse LPM particle resolution setup (e.g., $D_p = 0.5$ mm) where more fluctuations are spotted. In general, good agreement between LPM results and FEM results is found, and all predicted tip velocities are below the Rayleigh wave speed v_R of 2803 m/s.

3.2. Dynamic crack branching

Next, we intend to demonstrate the capability of the current method in simulating crack branching problems. Fig. 8 shows the geometrical detail and loading condition of the problem to be investigated in this example. Tensile stress applied at top and bottom edges of the rectangular plate is fixed at 1 MPa throughout the simulation. The material properties of the rectangular plate are [11]: Young's modulus $E = 32$ GPa, Poisson's ratio $\upsilon = 0.2$, density $\rho = 2450$ kg/m^3, material strength $\sigma_U = 4.5$ MPa and fracture energy $G_f = 3$ J/m^2. The initial notch in this problem is modelled by the Remove Bond (RB) method [35].

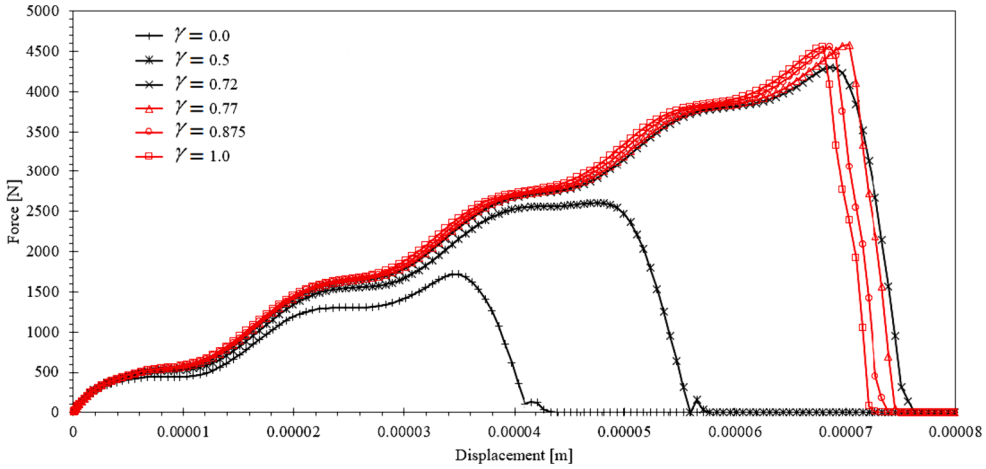

Fig. 17. Simulated force–displacement curves in the three-point bending test of John and Shah [57]. Force and displacement at the point where impact occurs are measured.

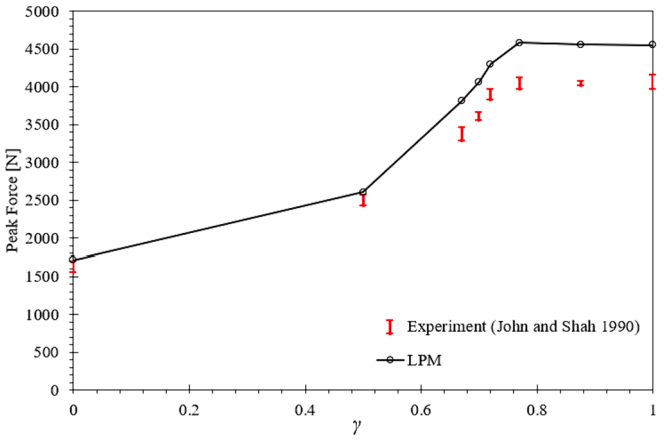

Fig. 18. Comparison of peak forces found during the impact of the three-point bending test of John and Shah [57].

The final crack paths predicted using different methods are shown in Fig. 9. As compared to FEM-local damage model [13], the damage zone along the crack path captured using the current approach is thicker, consistent to that simulated using the phase field approach [11]. This could be due to the lower material strength σ_U being considered in the current work and [11] as compared to that of [13] ($\sigma_U = 8$ MPa). Both the simulated upper and lower crack branches are symmetric to each other. Also, the crack patterns simulated using LPM with particle sizes $D_p = 0.25$ mm and $D_p = 0.125$ mm are almost indiscernible. The predicted crack branching angle as shown in Fig. 10 is quite close to the experimental observation [2] and the theoretical branching angle of 27° [55].

As recently reported by Bui and co-workers [13], the irregular finite element mesh with reasonable size should be employed for obtaining a physically meaningful result for this dynamic crack branching problem. According to them, asymmetric crack branching is observed when the relatively coarse unstructured mesh of size ~0.5 mm is used as shown in Fig. 11(b) (almost symmetric crack branching is captured when finer unstructured mesh size of ~0.3 mm is used [13]). Moreover, if structured finite element mesh is used (Fig. 11(c)), crack bifurcation would occur, and the crack might get arrested at one of the branches. Interestingly, by employing the current LPM model, a symmetric crack pattern can be obtained even by employing a structured (Cartesian) particle setup with coarse resolution of $D_p = 0.5$ mm (Fig. 11 (a)).

The dissipative energies during crack formation estimated using different methods are plotted in Fig. 12. Before crack branching, all the

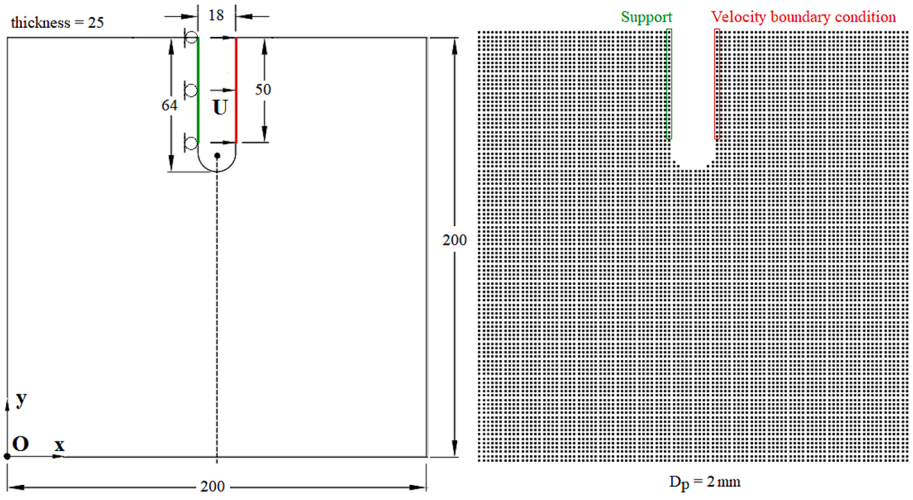

Fig. 19. Geometric details (dimensions in mm) of the compact tension test performed on a U-shape concrete specimen [59]. The LPM model with $D_p = 2$ mm is shown.

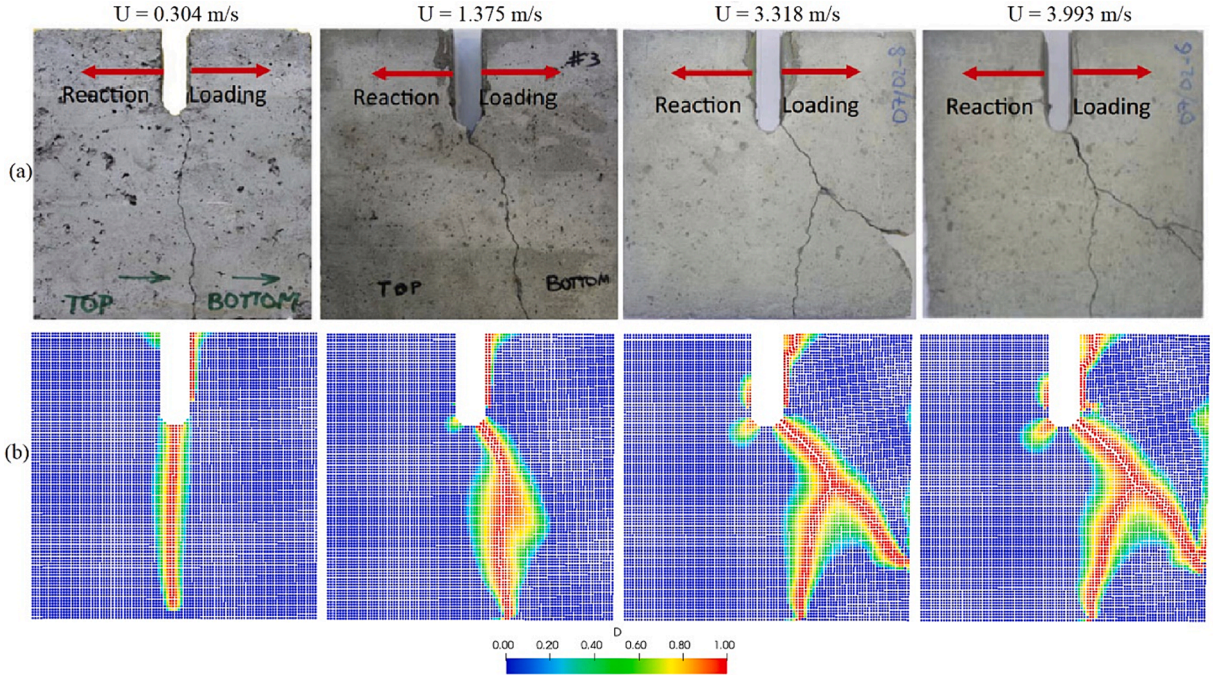

Fig. 20. Comparison of crack patterns predicted using LPM at different loading speed conditions against experiment [59]. The predicted crack patterns using LPM are captured at t = 1000 μs, except for U = 0.304 m/s at t = 500 μs.

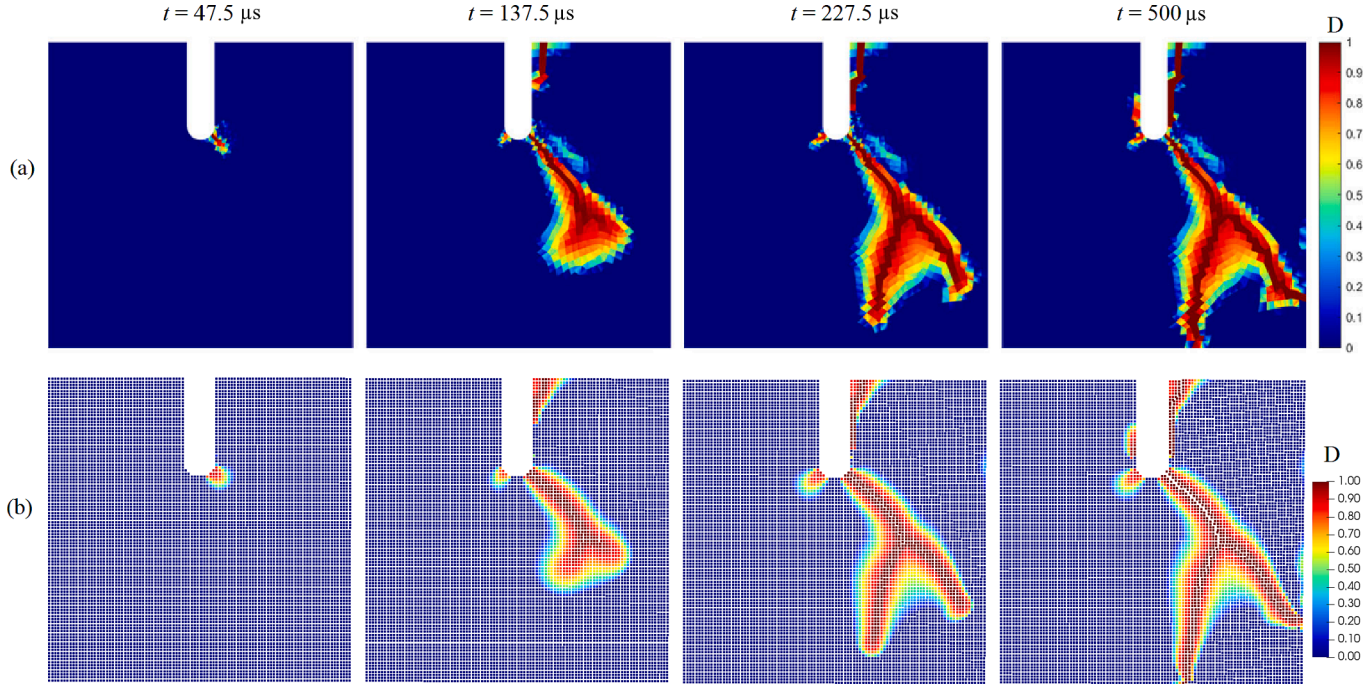

Fig. 21. Time evolution of damage field predicted using (a) FEM [13] and (b) LPM at loading speed U = 3.318 m/s.

estimated dissipative energies agree considerably well with each other. The effect of LPM particle size on the dissipative energy is also studied. It is found that the current LPM method shows marginal amount of particle size dependence in the dissipative energy. Fig. 13 shows the time evolution of the upper crack tip speed. It is appealing to note that our LPM results compare reasonably well with that from Ref. [13], albeit some wiggles are seen in the LPM solutions obtained using coarser particle resolution. In general, the estimated crack tip speeds within the time span considered are broadly below 60 % of the Rayleigh speed, which is agreeable with the phase field solution of Nguyen and Wu [56].

3.3. Mixed-Mode crack propagation in John-Shah Three-Point bending test

In this case, we intend to simulate the mixed-mode crack pattern observed in the three-point bending experiment which was previously performed by John and Shah [57]. The geometrical details of this problem are outlined in Fig. 14, where the notch location could be varied by manipulating the parameter γ to produce different crack pattern. Again, like the previous test case, the notch is modelled by the Remove Bond (RB) approach. Some possible crack paths are depicted in

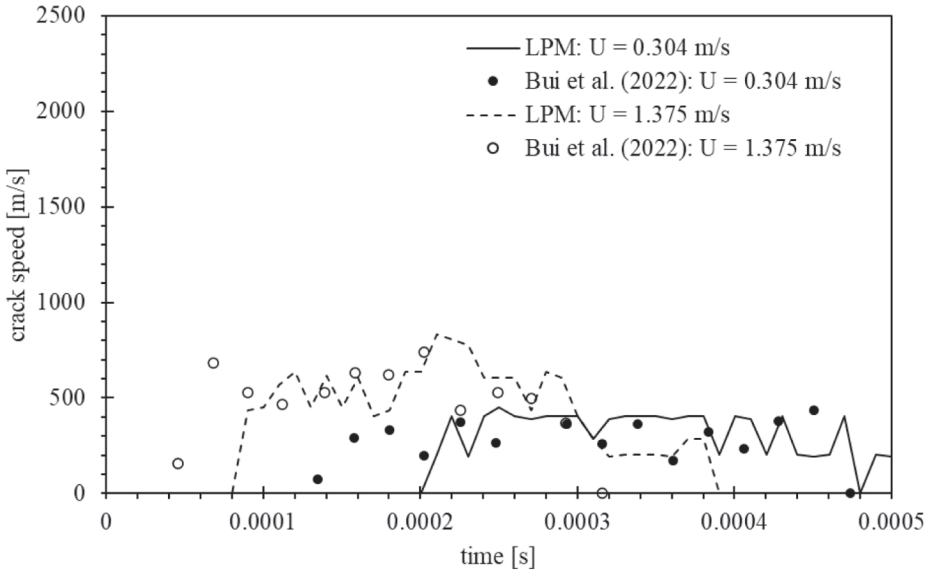

(a)

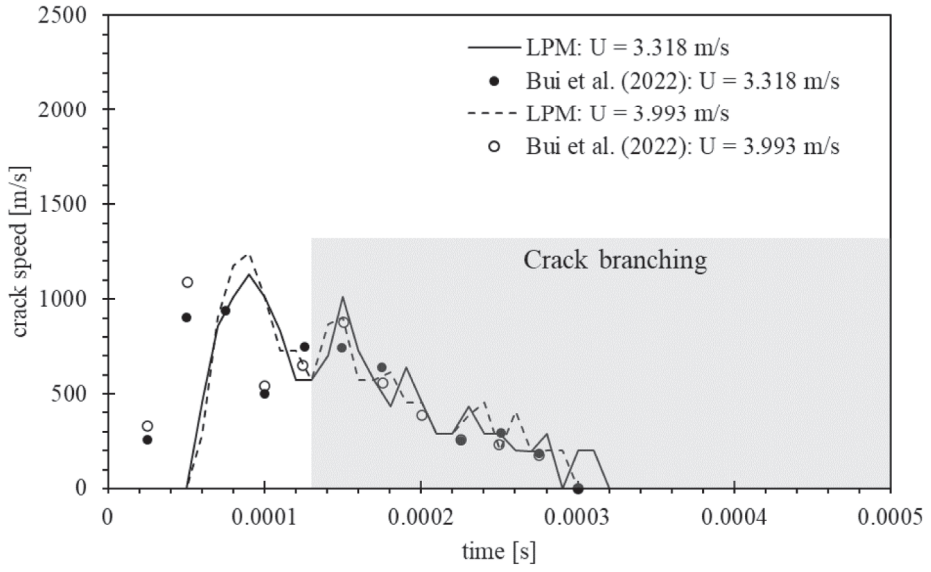

(b)

Fig. 22. Crack speeds predicted using LPM and FEM [13] for (a) low loading rate (U = 0.304 m/s and U = 1.375 m/s) and (b) high loading rate (U = 3.318 m/s and U = 3.993 m/s). For (b), crack speeds of the right branches are reported.

Fig. 15. When γ is less than the critical value γ_t, the crack grows from the notch. However, when the critical value is reached ($\gamma = \gamma_t$), cracks could be formed from the notch as well as the midspan. For larger values of γ such as $\gamma > \gamma_t$, crack propagates mainly from the midspan to the top edge of the specimen. It has been experimentally observed by John and Shah [57] that $\gamma_t \sim 0.77$.

In the current numerical simulation, the material properties are: Young's modulus $E = 28$ GPa, Poisson ratio $\upsilon = 0.2$, density $\rho = 2400$ kg/m^3, material strength $\sigma_U = 8$ MPa and fracture energy $G_f = 22$ J/m^2. Following [13], the particle size is set as 1 mm, and the impact velocity during the physical experiment is modelled using Eq. (19), where $t_o = 196$ μs and $v_o = 60$ mm/s. To obtain γ_t numerically, a series of cases with different γ values are simulated. Some results simulated using LPM are shown in Fig. 16 and it is found that $\gamma_t = 0.76$, which agrees considerably well with that reported experimentally [57]. The crack angles for $\gamma = 0.5$ and $\gamma = 0.72$ have been compared against those of LEFM [58] and good agreement has been found at least at the beginning stage when the crack starts to grow from the notch. Nevertheless, as the crack approaches the top edge, the simulated crack angle deviates from that of LEFM, and the crack bends towards the direction of the top loading point. Similar observation is reported by Belytschko and co-workers [58] upon comparing the LEFM solution against the experimentally observed crack patterns. Unlike the element-free Galerkin method [58], it is worth noting that in the current LPM simulation, the crack propagates from the

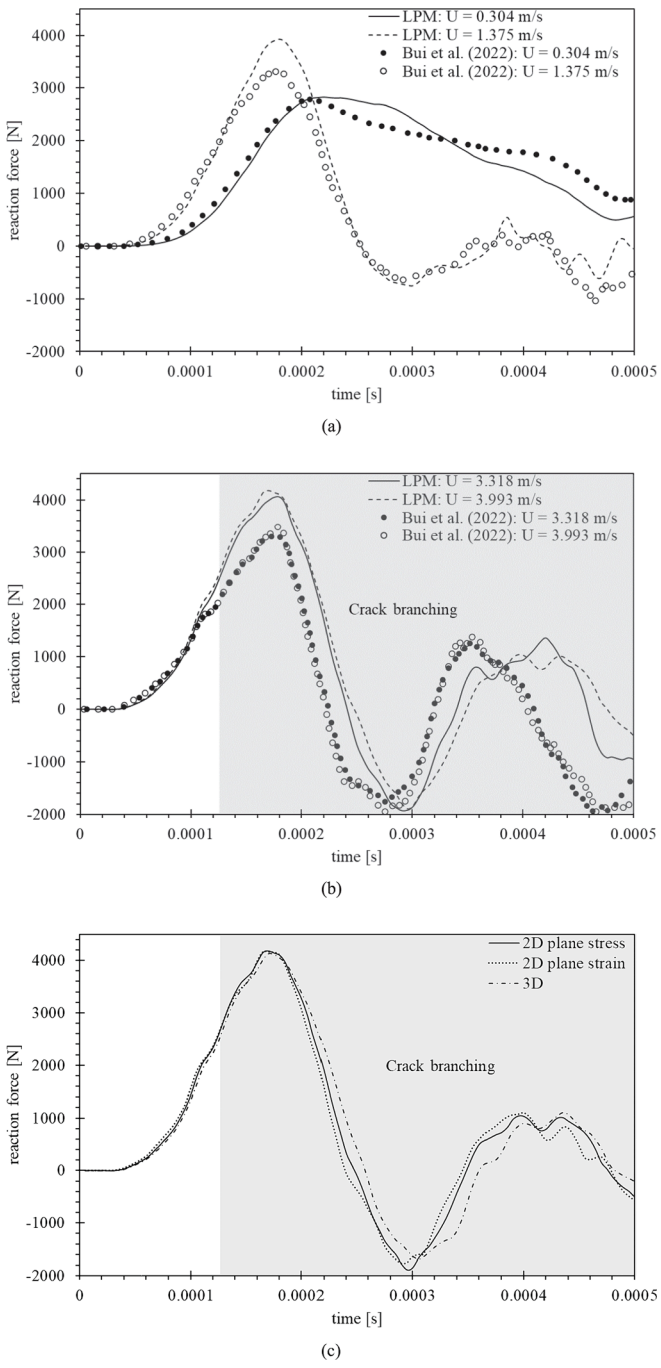

Fig. 23. Reaction forces predicted using LPM and FEM [13] for (a) low loading speed (U = 0.304 m/s and U = 1.375 m/s) and (b) high loading speed (U = 3.318 m/s and U = 3.993 m/s). For (c), 2D and 3D LPM results are shown for U = 3.993 m/s, where crack branches at t ~ 125 μs based on LPM result.

midspan naturally without introducing any small notch.

Fig. 17 shows the force–displacement curves for different initial notch locations. As the initial notch is located away from the midspan, the peak force increases and plateaus at a relatively constant value when $\gamma \geq 0.77$. Fig. 18 compares the experimental [57] and the simulated peak forces (using LPM). While the agreement is quite encouraging at low γ, the numerical error is getting more discernible as γ increases. Note that $\gamma = 0$ and $\gamma > 0$ corresponds to Mode-I and mixed mode fractures, respectively. For simulating mixed mode fracture accurately, instead of using the standard Rankine criterion, a more complex equivalent stress formulation might be required.

3.4. Dynamic fracture of concrete subjected to compact tension

Lastly, we intend to validate our LPM method by simulating the dynamic fracture in a real concrete specimen subjected to compact tension. This problem was initially studied by Ozbolt and co-workers [59] numerically and experimentally at different loading conditions. The loading condition and the geometrical details of this test case are depicted in Fig. 19, where the red edge is pulled with certain horizontal speed U and the green edge acts as a support. In the numerical setup, following [13], we apply Eq. (19) to model the loading condition by setting $t_o = 200$ μs and $v_o = 0.304$, 1.375, 3.318 and 3.993 m/s. Different U values are tested here as we intend to capture the change from mode-I fracture to mixed-mode fracture as U increases, which was observed experimentally [59]. The support is modelled by setting the horizontal velocities of the particles at the support domain as zeros. The material properties are: Young's modulus $E = 36$ GPa, Poisson ratio $\upsilon = 0.18$, density $\rho = 2400$ kg/m^3, material strength $\sigma_U = 3.8$ MPa and fracture energy $G_f = 65$ J/m^2. The particle size is fixed at 2 mm, which roughly corresponds to the mesh size in the refined zone near the notch [13].

Fig. 20 compares the predicted crack patterns using LPM against those captured experimentally at different loading rates. The simulated crack patterns agree considerably well with the experimental ones for all loading conditions. It is also interesting to note also that the change from mode-I fracture to mixed-mode fracture (including the crack branching) as the loading rate is higher is well captured using the current LPM method. The dynamic fracture patterns for $U = 3.318$ m/s at different time levels have been compared against those of FEM [13] and the results are presented in Fig. 21. As seen, the agreement between both sets of numerical results is promising at all time levels.

Next, the calculated crack speeds using LPM are compared against those of FEM [13] for low and high loading rates as shown in Fig. 22. Specifically, at low loading rate ($U = 0.304$ m/s and $U = 1.375$ m/s), no crack branching is found, and the crack tip speed is almost uniform upon the crack formation from the circular arc. At high loading rates ($U = 3.318$ m/s and $U = 3.993$ m/s), the crack tip speed decays almost linearly upon the crack branching event occurred at $t \sim 125$ μs. In general, the current LPM results agree generally well with those of FEM, except that the latter suggests an earlier crack nucleation.

The time history of the reaction force at the support is recorded and the result is compared against those of FEM [13] as shown in Fig. 23. Here, the reaction force is obtained by the expression: $\sum_G \sigma_{xx} \Delta A$ where G is the support region (see Fig. 19) and ΔA is the differential area of each LPM particle ($\Delta A = t_h \times D_P$ for 2D, where $t_h = 25$ mm is the thickness). At low loading rates, the LPM results agree quite well with those of FEM in general, except that the estimated peak force for the $U = 1.375$ m/s case using LPM is higher than that of FEM. At high loading rates, the agreement between both LPM and FEM results is good before crack branching occurs. After crack branching, it seems that there is a phase lag between both sets of numerical results. The effect of 2D plane strain and 3D LPM models on the reaction force for the highest loading rate ($U = 3.993$ m/s) is studied as well. In general, the results are almost similar between all LPM modelling approaches, with more discrepancy is found after the crack branches. The respective crack patterns at $t \sim 500$ μs using different LPM modelling approaches are depicted in Fig. 24 and the results show no significant difference between each other.

4. Conclusion

In this study, a local damage model has been developed for the Lattice Particle Method (LPM) for simulating dynamic fracture. To verify and validate the developed model, several benchmark examples have been studied, and good agreements have been found with both experimental observations and numerical results obtained using other numerical models. Based on the numerical results obtained from the current work, some key conclusions can be summarized as below:

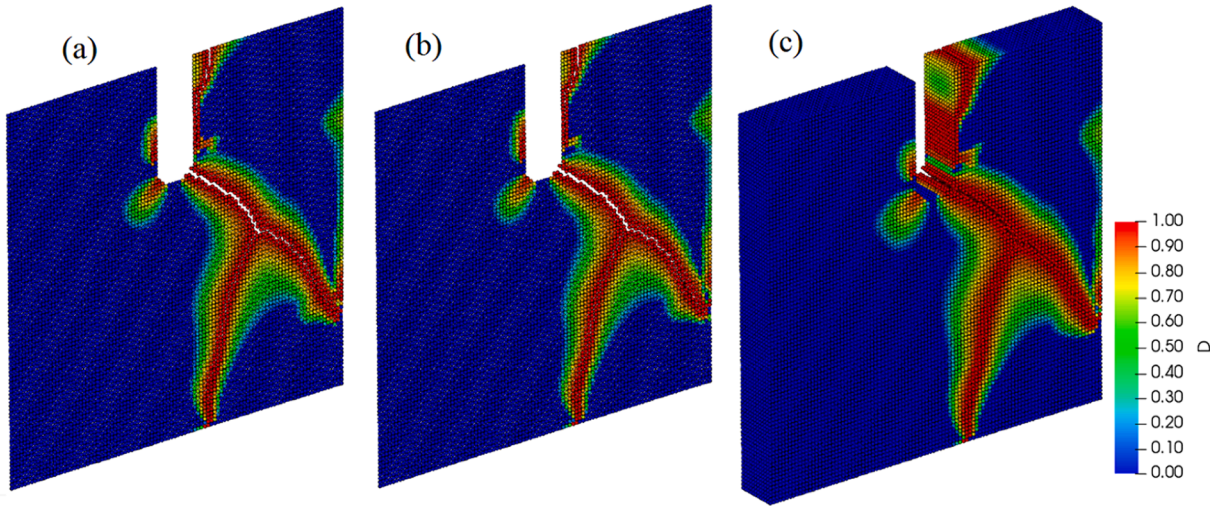

Fig. 24. Predicted crack patterns at $t = 500$ μs using (a) 2D plane stress; (b) 2D plane strain and (c) 3D LPM models. $U = 3.993$ m/s.

- By developing the local damage model in LPM, we have successfully simulated dynamic brittle and quasi-brittle fractures of various modes. Different from our previous fracture model based on mode-I Stress Intensity Factor (SIF) for LPM, the current model is more robust as it can handle problems with multiple cracks and under mixed-mode. By using the force formulation developed in the current work, a bond connecting two LPM particles is intrinsically "damaged" (hence it carries zero load) when the damage values of two interacting particles approach 1.0. Unlike some FEM models where damaged elements might be deleted (when the damage value exceeds a preset threshold) for numerical stability purpose [60], no special treatment (e.g., bond deletion) is needed for ensuring the numerical stability of the current LPM method.
- The method can produce particle size independent solution by employing a simple local damage description based on fracture mechanics. Quantities such as dissipative energy and crack tip speed at different time steps have been compared against the theoretical and other numerical solutions and good agreement has been found. For the Kalthoff-Winkler dynamic fracture case, the simulated dissipative energy using LPM is very close to the theoretical solution.
- Most FEM procedures rely on the use of unstructured mesh to get rid of the mesh-bias issue. Otherwise, some advanced numerical treatments such as crack tracking, non-local strain averaging, etc. are needed. In the current LPM approach, although a structured particle layout (square lattice for 2D and cubic lattice for 3D) is employed, a physically meaningful crack pattern can still be obtained without any special numerical treatment.

Using the current local damage model, we have extended the capability of LPM in simulating challenging dynamic brittle and quasi-brittle fracture problems with complex crack patterns in a more convincing manner. In future, a collision model is undoubtedly required to model the possible collision between two newly formed fractured surfaces. In this regard, a bond between two "damaged" particles could be deleted and replaced it with a DEM bond. The implementation of other more advanced yield surfaces could be needed to simulate more challenging mixed-mode fracture problems subjected to more complex loading conditions. Furthermore, the effect of random nature of the spatial distribution of material properties can be directly incorporated into the present method for studying fracture in real material.

CRediT authorship contribution statement

K.C. Ng: Conceptualization, Data curation, Formal analysis, Funding acquisition, Investigation, Methodology, Project administration, Resources, Software, Supervision, Validation, Visualization, Writing – original draft, Writing – review & editing. **Hailong Chen:** Supervision, Writing – original draft. **W.C. Low:** Investigation.

Declaration of competing interest

The authors declare that they have no known competing financial interests or personal relationships that could have appeared to influence the work reported in this paper.

Data availability

Data will be made available on request.

Acknowledgement

The financial supports given by Ministry of Higher Education (MoHE), Malaysia under the Fundamental Research Grant Scheme: FRGS/1/2021/TK0/UNIM/02/6 is greatly acknowledged. The first author would like to thank Dr. Alejandro Cornejo for his guidance on the local damage model implemented in the current work.

References

[1] K. Ravi-Chandar, 2.05 - Dynamic Fracture, in: Comprehensive Structural Integrity: Nine Volume Set, vol. 1–9, 2003. doi: 10.1016/B0-08-043749-4/02120-0.
[2] M. Ramulu, A.S. Kobayashi, Mechanics of crack curving and branching - a dynamic fracture analysis, Int. J. Fract. 27 (3–4) (1985) 187–201, https://doi.org/10.1007/BF00017967.
[3] J.F. Kalthoff, Modes of dynamic shear failure in solids, Int. J. Fract. 101 (2000) 1–31.
[4] N. Moës, J. Dolbow, T. Belytschko, A finite element method for crack growth without remeshing, Int. J. Numer. Methods Eng. 46(1) (1999), doi: 10.1002/(SICI)1097-0207(19990910)46:1<131::AID-NME726>3.0.CO;2-J.
[5] M. Cervera, G.B. Barbat, M. Chiumenti, Finite element modeling of quasi-brittle cracks in 2D and 3D with enhanced strain accuracy, Comput. Mech. 60 (5) (2017) 767–796, https://doi.org/10.1007/s00466-017-1438-8.
[6] J. Oliver, M. Cervera, S. Oller, Isotropic Damage Models and Smeared Crack Analysis of Concrete. Second International Conference on Computer Aided Analysis and Design of Concrete Structures, SCI-C'90, Zell am See, Austria, 1990.
[7] R.H.J. Peerlings, R. De Borst, W.A.M. Brekelmans, J.H.P. De Vree, Gradient enhanced damage for quasi-brittle materials, Int. J. Numer. Methods Eng. 39 (19) (1996) doi: 10.1002/(SICI)1097-0207(19961015)39:19<3391::AID-NME7>3.0.CO;2-D.
[8] T.H.A. Nguyen, T.Q. Bui, S. Hirose, Smoothing gradient damage model with evolving anisotropic nonlocal interactions tailored to low-order finite elements, Comput. Methods Appl. Mech. Eng. 328 (2018), https://doi.org/10.1016/j.cma.2017.09.019.
[9] M. Jirásek, B. Patzák, Consistent tangent stiffness for nonlocal damage models, Comput. Struct. 80 (14–15) (2002) pp, https://doi.org/10.1016/S0045-7949(02)00078-0.

[10] P. Grassl, M. Jirásek, Plastic model with non-local damage applied to concrete, Int. J. Numer. Anal. Meth. Geomech. 30 (1) (2006), https://doi.org/10.1002/nag.479.
[11] M.J. Borden, C.V. Verhoosel, M.A. Scott, T.J.R. Hughes, C.M. Landis, A phase-field description of dynamic brittle fracture, Comput. Methods Appl. Mech. Eng. 217–220 (2012) 77–95, https://doi.org/10.1016/j.cma.2012.01.008.
[12] R.J.M. Geelen, Y. Liu, T. Hu, M.R. Tupek, J.E. Dolbow, A phase-field formulation for dynamic cohesive fracture, Comput. Methods Appl. Mech. Eng. 348 (2019) 680–711, https://doi.org/10.1016/j.cma.2019.01.026.
[13] T.Q. Bui, H.T. Tran, X. Hu, C.-T. Wu, Simulation of dynamic brittle and quasi-brittle fracture: a revisited local damage approach, Int. J. Fract. 236 (1) (2022) 59–85, https://doi.org/10.1007/s10704-022-00635-1.
[14] Z.P. Bažant, B.H. Oh, "Crack band theory for fracture of concrete", Matériaux et, Constructions 16 (3) (1983) pp, https://doi.org/10.1007/BF02486267.
[15] A. Hillerborg, M. Modéer, P.E. Petersson, Analysis of crack formation and crack growth in concrete by means of fracture mechanics and finite elements, Cem. Concr. Res. 6 (6) (1976) pp, https://doi.org/10.1016/0008-8846(76)90007-7.
[16] M. Kurumatani, K. Terada, J. Kato, T. Kyoya, K. Kashiyama, An isotropic damage model based on fracture mechanics for concrete, Eng. Fract. Mech. 155 (2016), https://doi.org/10.1016/j.engfracmech.2016.01.020.
[17] M. Cervera, L. Pelà, R. Clemente, P. Roca, A crack-tracking technique for localized damage in quasi-brittle materials, Eng. Fract. Mech. 77 (13) (2010) pp, https://doi.org/10.1016/j.engfracmech.2010.06.013.
[18] X. Li, W. Gao, W. Liu, A mesh objective continuum damage model for quasi-brittle crack modelling and finite element implementation, Int. J. Damage Mech 28 (9) (2019), https://doi.org/10.1177/1056789518823876.
[19] Y.D. Ha, F. Bobaru, Studies of dynamic crack propagation and crack branching with peridynamics, Int. J. Fract. 162 (1–2) (2010) 229–244, https://doi.org/10.1007/s10704-010-9442-4.
[20] F. Bobaru, G. Zhang, Why do cracks branch? A peridynamic investigation of dynamic brittle fracture, Int. J. Fract. 196 (1–2) (2015) 59–98, https://doi.org/10.1007/s10704-015-0056-8.
[21] S.A. Silling, E. Askari, A meshfree method based on the peridynamic model of solid mechanics, Comput. Struct. (2005), https://doi.org/10.1016/j.compstruc.2004.11.026.
[22] Y. Zhao, Z. Zhou, J. Bi, C. Wang, Simulation of brittle fractures using energy-bond-based smoothed particle hydrodynamics, Int. J. Mech. Sci. 248 (2023), https://doi.org/10.1016/j.ijmecsci.2023.108236.
[23] M. Rushdie, I. Islam, C. Peng, A Total Lagrangian SPH Method for Modelling Damage and Failure in Solids, Int. J. Mech. Sci. 157–158 (2019) 498–511.
[24] S. Hentz, L. Daudeville, F.V. Donzé, Identification and validation of a discrete element model for concrete, J. Eng. Mech. 130(6) (2004) doi: 10.1061/(asce)0733-9399(2004)130:6(709).
[25] L.F. Orozco, J.Y. Delenne, P. Sornay, F. Radjai, Discrete-element model for dynamic fracture of a single particle, Int. J. Solids Struct. 166 (2019), https://doi.org/10.1016/j.ijsolstr.2019.01.033.
[26] G.F. Zhao, J. Fang, J. Zhao, A 3D distinct lattice spring model for elasticity and dynamic failure, Int. J. Numer. Anal. Meth. Geomech. 35 (8) (2011) pp, https://doi.org/10.1002/nag.930.
[27] G.F. Zhao, Developing a four-dimensional lattice spring model for mechanical responses of solids, Comput. Methods Appl. Mech. Eng. 315 (2017), https://doi.org/10.1016/j.cma.2016.11.034.
[28] H. Chen, E. Lin, Y. Liu, A novel Volume-Compensated Particle method for 2D elasticity and plasticity analysis, Int. J. Solids Struct. 51 (9) (2014) 1819–1833, https://doi.org/10.1016/j.ijsolstr.2014.01.025.
[29] Z. Pan, R. Ma, D. Wang, A. Chen, A review of lattice type model in fracture mechanics: theory, applications, and perspectives, Eng. Fract. Mech. 190 (2018), https://doi.org/10.1016/j.engfracmech.2017.12.037.
[30] J.X. Liu, Z.Y. Zhao, S.C. Deng, N.G. Liang, Modified generalized beam lattice model associated with fracture of reinforced fiber/particle composites, Theor. Appl. Fract. Mech. 50 (2) (2008) pp, https://doi.org/10.1016/j.tafmec.2008.07.006.
[31] G. Lilliu, J. G. M. van Mier, 3D lattice type fracture model for concrete, Eng. Fract. Mech. 70(7–8), 2003, doi: 10.1016/S0013-7944(02)00158-3.
[32] H. Chen, Y. Liu, A non-local 3D lattice particle framework for elastic solids, Int. J. Solids Struct. 81 (2016) 411–420, https://doi.org/10.1016/j.ijsolstr.2015.12.026.
[33] C. Meng, Y. Liu, Damage-augmented nonlocal lattice particle method for fracture simulation of solids, Int. J. Solids Struct. 243 (2022), https://doi.org/10.1016/j.ijsolstr.2022.111561.
[34] J.E. Bolander, J. Eliáš, G. Cusatis, K. Nagai, Discrete mechanical models of concrete fracture, Eng. Fract. Mech. 257 (2021), https://doi.org/10.1016/j.engfracmech.2021.108030.
[35] K.C. Ng, H. Chen, Numerical modelling of brittle fracture using lattice particle method with applications to fluid structure interaction problems via SPH coupling, Eng. Fract. Mech. 289 (2023), https://doi.org/10.1016/j.engfracmech.2023.109453.
[36] H. Chen, E. Lin, Y. Jiao, Y. Liu, A generalized 2D non-local lattice spring model for fracture simulation, Comput. Mech. 54 (6) (2014) 1541–1558, https://doi.org/10.1007/s00466-014-1075-4.
[37] K.C. Ng, A. Alexiadis, H. Chen, T.W.H. Sheu, A coupled smoothed particle hydrodynamics-volume compensated particle method (SPH-VCPM) for fluid structure interaction (FSI) modelling, Ocean Eng. 218 (2020), https://doi.org/10.1016/j.oceaneng.2020.107923.
[38] K.C. Ng, A. Alexiadis, H. Chen, T.W.H. Sheu, Numerical computation of fluid–solid mixture flow using the SPH–VCPM–DEM method, J. Fluids Struct. 106 (2021) 103369.
[39] K.C. Ng, A. Alexiadis, Y.L. Ng, An improved particle method for simulating Fluid-Structure Interactions: the multi-resolution SPH-VCPM approach, Ocean Eng. 247 (January) (2022) 110779, https://doi.org/10.1016/j.oceaneng.2022.110779.
[40] B. Choo, J. W. Park, Y. J. Nam, Y. K. Hwang, Y. M. Lim, Mesh-size independent rigid-body spring network for simulation of the dynamic fracture behavior of concrete, Int. J. Numer. Anal. Methods Geomech. 47(5) (2023), doi: 10.1002/nag.3497.
[41] W.C. Low, K.C. Ng, H.K. Ng, A SPH-lattice spring method for modelling Fluid Structure Interaction involving composite body and free surface, Comput. Part. Mech. (2023), https://doi.org/10.1007/s40571-023-00576-z.
[42] M. Cervera, M. Chiumenti, Mesh objective tensile cracking via a local continuum damage model and a crack tracking technique, Comput. Methods Appl. Mech. Eng. 196 (1–3) (2006) 304–320, https://doi.org/10.1016/j.cma.2006.04.008.
[43] P. Sun, Y. Cai, H. Zhu, A simple approach for pervasive quasi-brittle fracture using independent cover meshless method, Theor. Appl. Fract. Mech. 108 (2020), https://doi.org/10.1016/j.tafmec.2020.102600.
[44] Y. K. Hwang, S. Jin, J. W. Hong, Fracture simulations using edge-based smoothed finite element method for isotropic damage model via Delaunay/Voronoi dual tessellations, Int. J. Damage Mech. 31(3) (2022), doi: 10.1177/10567895211040549.
[45] F. Zárate, E. Oñate, A simple FEM–DEM technique for fracture prediction in materials and structures, Comput. Part Mech. 2(3) (2015), doi: 10.1007/s40571-015-0067-2.
[46] V.C. Li, C.-M. Chan, C.K.Y. Leung, Experimental determination of the tension-softening relations for cementitious composites, Cem. Concr. Res. 17 (3) (1987) 441–452, https://doi.org/10.1016/0008-8846(87)90008-1.
[47] J.H. Song, T. Belytschko, Cracking node method for dynamic fracture with finite elements, Int. J. Numer. Meth. Eng. 77 (3) (2009) 360–385, https://doi.org/10.1002/nme.2415.
[48] K.C. Ng, W.C. Low, H. Chen, A. Tafuni, A. Nakayama, A three-dimensional fluid-structure interaction model based on SPH and lattice-spring method for simulating complex hydroelastic problems, Ocean Eng. 260 (2022) 112026, https://doi.org/10.1016/j.oceaneng.2022.112026.
[49] H. Chen, Constructing continuum-like measures based on a nonlocal lattice particle model: Deformation gradient, strain and stress tensors, Int. J. Solids Struct. 169 (2019) 177–186, https://doi.org/10.1016/j.ijsolstr.2019.04.014.
[50] C. Meng, H. Wei, H. Chen, Y. Liu, Modeling plasticity of cubic crystals using a nonlocal lattice particle method, Comput. Methods Appl. Mech. Eng. 385 (2021), https://doi.org/10.1016/j.cma.2021.114069.
[51] S. Chakraborty, A. Shaw, A pseudo-spring based fracture model for SPH simulation of impact dynamics, Int. J. Impact Eng 58 (2013) 84–95, https://doi.org/10.1016/j.ijimpeng.2013.03.006.
[52] Y.J. Lee, L.B. Freund, Fracture initiation due to asymmetric impact loading of an edge cracked plate, J. Appl. Mech. Trans. ASME 57 (1) (1990) 104–111, https://doi.org/10.1115/1.2888289.
[53] K.V. Ganesh, M.R.I. Islam, P.K. Patra, K.P. Travis, A pseudo-spring based SPH framework for studying fatigue crack propagation, Int. J. Fatigue 162 (2022) 106986, https://doi.org/10.1016/J.IJFATIGUE.2022.106986.
[54] M.N. Rahimi, D.C. Kolukisa, M. Yildiz, M. Ozbulut, A. Kefal, A generalized hybrid smoothed particle hydrodynamics–peridynamics algorithm with a novel Lagrangian mapping for solution and failure analysis of fluid–structure interaction problems, Comput. Methods Appl. Mech. Eng. 389 (2022) 114370, https://doi.org/10.1016/j.cma.2021.114370.
[55] E. Katzav, M. Adda-Bedia, R. Arias, Theory of dynamic crack branching in brittle materials, Int. J. Fract. 143 (3) (2007) 245–271, https://doi.org/10.1007/s10704-007-9061-x.
[56] V.P. Nguyen, J.-Y. Wu, Modeling dynamic fracture of solids with a phase-field regularized cohesive zone model, Comput. Methods Appl. Mech. Eng. 340 (2018) 1000–1022, https://doi.org/10.1016/j.cma.2018.06.015.
[57] R. John, S.P. Shah, Mixed-mode fracture of concrete subjected to impact loading, J. Struct. Eng. (United States) 116 (3) (1990) 585–602, https://doi.org/10.1061/(ASCE)0733-9445(1990)116:3(585).
[58] T. Belytschko, D. Organ, C. Gerlach, Element-free galerkin methods for dynamic fracture in concrete, Comput. Methods Appl. Mech. Eng. 187 (3–4) (2000) 385–399, https://doi.org/10.1016/S0045-7825(00)80002-X.
[59] J. Ožbolt, J. Bošnjak, E. Sola, Dynamic fracture of concrete compact tension specimen: experimental and numerical study, Int. J. Solids Struct. 50 (25–26) (2013) 4270–4278, https://doi.org/10.1016/j.ijsolstr.2013.08.030.
[60] Z. Alomar, C. Cappellini, F. Concli, An element deletion algorithm for an open-source finite element software, Lect. Notes Mech. Eng. (2022), https://doi.org/10.1007/978-3-031-06025-0_14.